The cooling efficiency of s-CO₂ microchannel heat sink compared with a water-based design

Dehdashti Akhavan, Navid; Abroug, Foued; Arnaud, Lionel; Hooman, Kamel

Citation (APA)
Dehdashti Akhavan, N., Abroug, F., Arnaud, L., & Hooman, K. (2022). The cooling efficiency of s-CO₂ microchannel heat sink compared with a water-based design. *Mathematical Methods in the Applied Sciences*, *46 (2023)*(10), 11666-11682. https://doi.org/10.1002/mma.8535

Important note
To cite this publication, please use the final published version (if applicable).
Please check the document version above.

SPECIAL ISSUE PAPER

WILEY

The cooling efficiency of s-CO$_2$ microchannel heat sink compared with a water-based design

Navid Dehdashti Akhavan[1] | **Foued Abroug[2]** | **Lionel Arnaud[2]** | **Kamel Hooman[3]**

[1]School of Mechanical and Mining Engineering, The University of Queensland, Brisbane, Queensland, Australia

[2]Laboratoire Génie de Production (LGP), Université de Toulouse, INP-ENIT, Tarbes, France

[3]Faculty of Mechanical Engineering, Technische Universiteit Delft, Delft, The Netherlands

Correspondence

Navid Dehdashti Akhavan, Department of Mechanical and Mining Engineering, The University of Queensland, Brisbane, QLD, Australia.
Email: navid.dehdashti@uqconnect.edu.au

High-pressure drops characteristic of microchannel heat sinks (MCHS) is an issue that needs to be addressed to reduce the size of heat-removing devices in compact electronic devices. Supercritical carbon dioxide (s-CO$_2$) is a suitable candidate being proposed as an alternative coolant to enhance the cooling of the microchannel heat sink (MCHS), with high heat flux, due to its favorable thermophysical properties near its critical point. In this study, numerical simulations are conducted to evaluate the thermal and hydraulic performance of a channel for a designed heat sink with s-CO$_2$ (at constant $P = 8\,\text{MPa}$) and compare it with conventional liquid coolant (water). The effect of coolants mass flow rate ($\dot{m}$), channel aspect ratio (AR), and inlet temperatures on the thermal and hydraulic performance of one channel is studied by varying $\dot{m}$ from 0.004 to 0.03 kg/s and AR from 0.33 to 10. The results show that, for the same aspect ratio, same geometry, and constant heat flux, s-CO$_2$ offers a higher overall heat transfer coefficient (32%) with a lower friction factor (pumping power) compared with the water at the same inlet temperature (T $= 32°$C). The results of pumping power comparison between two coolants reveal that for CO$_2$ in supercritical conditions ($P = 8\,\text{MPa}$, T $= 32°$C), the consumed power varies by change of the aspect ratio, which is 1.85 times lower than water for AR $= 0.33$ and is 3.6 times higher for AR $= 10$. However, in the subcooled state, the reverse effect of the aspect ratio is seen.

KEYWORDS
CFD, electronic cooling, heat sink, IGBT, pumping power, s-CO$_2$

1 | INTRODUCTION

A wide range of applications of cooling systems in thermal engineering is recognized and studied both theoretically and practically in areas such as electronic devices, micropower generation, computer chips, biomedical use, and many more. Increasingly, thermal management of electronic devices has become a critical topic as new generations of high-performing chip packages requiring high frequencies produce very high heat fluxes. As explained in Black's

equation, a prolonged heat flux results in a hot spot on the electronic device, reducing device lifespan because the meantime to failure (MTTF) accelerates.[1]

Compact electronic devices that operate at high power densities require proper thermal management, as there are no effective techniques for removing heat dissipation from these devices.[2] With the increase in power density and miniaturization of electronic packages, cooling system technology has changed from air-cooling technology to advanced heat transfer technology as conventional methods are insufficient to remove extreme, high heat flux.[3] Liquid-cooled micro-channels are capable of minimizing maximum substrate temperatures and reducing gradients of substrate temperatures in electronics cooling which are two key objectives in electronic cooling. Because of its high heat transfer surface area to volume ratio, the cooled micro-channels heat sink (MCHS) can dissipate considerable heat generated by compact electronic devices. Furthermore, the micro hydraulic diameter also maximizes heat transfer by enhancing the heat transfer coefficient.[4] As Tuckerman and Pease reported,[5] a rectangular MCHS can remove heat flux up to 790 W/cm^2, but the amount of pumping power required by the MCHS is very high due to the high pressure drop penalty in the microchannel. Japar et al.[6] study suggested that high wall shear stress in the developing laminar flow region is responsible for high-pressure drop penalty. This became the motivation of many researchers to examine the performance of rectangular microchannel by modifying geometry parameters. Moreover, researchers[7–9] have shown that by increasing the aspect ratio (channel width to channel height) of the rectangular microchannel, thermal and hydraulic resistances decreased as a result of larger convective heat transfer areas and flow cross sections, respectively. It was also found that channel width, with a fixed aspect ratio, affected thermal resistance significantly since the bottom part of the channels sat directly below the heat flux. Additionally to the thermal resistance issue, the rectangular channel MCHS optimization process also targeted the pressure drop penalty.

Hydrothermal has recently been further improved through the application of nanotechnology. Several experiments and studies have recently been conducted to enhance the performance of MCHS and fluid between parallel plates through advanced geometric structure and nanofluids, which facilitate high thermal and hydraulic performance but at the cost of excessive pressure drop.[10–12]

In addition to the abovementioned methods, the use of a suitable heat transfer fluid is another option to improve the thermal performance of MCHS. There are a number of criteria to take into account when choosing a heat transfer liquid, including performance, operating range, temperature range, and chemical stability. Therefore, a new type of coolant is needed for heat removing systems that can dissipate heat well without causing pressure losses. In this regard, we propose supercritical CO_2 (s-CO_2) for electronic cooling via MCHS in the current study.

For the last two decades, thermohydraulics of supercritical carbon dioxide (s-CO_2) as a cooling fluid have been investigated in the anticipation of compact s-CO_2 heat exchangers and turbomachinery. Accordingly, a great deal of information is available on s-CO_2 as working and heat transfer fluid for various applications such as refrigeration and air-conditioning systems, solar thermal, nuclear, and waste heat recovery plants.[1–3,13,14] A supercritical Rankine system that utilizes low-grade heat was also proposed using this working fluid.[4,15,16] Apart from its environmentally friendly nature, availability, chemical stability, non-toxic, and non-flammable nature, s-CO_2 has excellent thermophysical properties near its critical point (T = 304 K, P = 7.34 MPa), which makes it a great candidate to be used as coolant in MCHS. s-CO_2 can also solve problems associated with liquid coolants, such as short circuits caused by leaked coolants and nanoparticles clogging heatsink channels. Even though the technology of s-CO_2 systems has improved in power generation, heating ventilation, air conditioning (HVAC), and automotive industries, the viability of using s-CO_2 in other applications is still under investigation by researchers.[14,17,18] Interesting experimental studies have already been conducted to prove the high efficiency of CO_2 in refrigeration cycles, in both subcritical and supercritical regions.[6–8] These studies are focusing on s-CO_2 as coolant and cover a variety of channel geometries and operating temperature ranges.

Channels are used in heat sinks to move the coolant around, control flow distribution, and enhance (local) cooling performance of the system. The geometry of channels, which is a very crucial parameter in determining the performance of the heat sink, is categorized from conventional to micro-channel considering their hydraulic diameters. Mehendal et al.[16] and Kandlikar et al.[19] have proposed different classifications as shown in Table 1.

Since the introduction of MCHS by Tuckerman and Pease,[20] many researchers have studied the performance of MCHS with water and air to optimize the geometry of the channel and increase the heat transfer.[17,18]

In parallel, few studies have considered MCHS using other exotic coolants such as s-CO_2.[21,22] Sarkar[23] has carried out an energy analysis of a MCHS similar to the one used by Tamura et al.[5] and compared its thermal performance for water and s-CO_2 for constant heat flux of 300 W/cm^2 and flow rate of 10 cm^3/s. His results showed that the s-CO_2 yields

TABLE 1 Classification of channels according to previous studies[16,19]

Mehendale		Kandlikar	
Conventional channels	$D_h > 6$ mm	Conventional channel	$D_h > 3$ mm
Compact passages	$1 < D_h < 6$	Mini-channels	$200\,\mu m < D_h < 3$ mm
Meso-channels	$100\,\mu m < D_h < 1$ mm	Micro-channels	$10\,\mu m < D_h < 200\,\mu m$
Micro-channels	$1\,\mu m < D_h < 100$ mm	Transitional channels	$0.1\,\mu m < D_h < 10\,\mu m$
		Molecular nano-channels	$D_h < 0.1\,\mu m$

lower thermal resistance for a certain range of fluid inlet temperature values. But he did not consider the effect of thermal and hydraulic entrance length on the heat transfer performance as discussed earlier. On the other hand, both thermal resistance and pumping power were highly dependent on s-CO_2 inlet pressure and temperature, which highlights the importance of the heat source temperature as a key design parameter.[18]

The field of cooling plates for electronic components continues to witness innovation. The number of related patented applications is in a continuous increase.[24] Among other reasons, the recent development in additive manufacturing techniques has opened numerous prospects for the optimization of heat exchangers, and more companies are rapidly developing skills in these techniques.[25]

The present study will address two objectives, which, to the best of the authors' knowledge, have not been explicitly investigated in other published reports. First, the thermal performance of a specifically designed heat sink, using two different cooling fluids, namely, water and s-CO_2, is investigated. The main variables such as heat transfer and pumping power and the thermal performance of each cooling fluid are presented through graphs. The second objective of the study is to perform a sensitivity analysis of key variables such as Reynolds number, aspect ratio, and entrance length (thermal and hydraulic) since they have significant effect on the cooling performance of the heat sink for each of the cooling fluids under constant heat flux. It is shown that the heat transfer and pumping power in heat sinks are highly dependent on these variables, which have not been sufficiently addressed in the previous literatures. Therefore, results are depicted on graphs for a better understanding of the scientific community and engineers to assist them in improving their designs.

The numerical study is carried out based on CFD analysis using commercial software ANSYS Fluent ® and the main advantages of each cooling fluid are elaborated and conclusions are drawn.

1.1 | Characteristics of s-CO_2

With pressure and temperature exceeding those of critical values, the fluid is called supercritical. For CO_2, the critical values are $P = 7.38$ MPa and T $= 304.25$ K.[13] In the vicinity of the pseudo-critical temperature, rapid changes of the CO_2 thermo-physical properties make its heat transfer characteristics complex and unique.[13] Such phenomena result in an interesting thermohydraulic performance as a result of high specific heat and low-pressure drop. Figure 1 illustrates the thermal properties of s-CO_2 at 8 MPa. As shown, specific heat (Cp) of s-CO_2, near the critical region, is about 29 kJ/kg K, which is six times higher than that of water. This feature is one of the obvious reasons, which makes s-CO_2 an attractive substitute to water in heat transfer applications. However, in the case of heat sinks, these characteristics can be highly affected by other parameters such as inlet pressure, temperature, mass flux, heat flux, and channel diameter.[24] The effects of these parameters on the overall performance of the heat sink will be numerically studied in this paper.

2 | COMPUTATIONAL MODELING

In this study, the cooling performance of a heated channel is compared by using two different cooling fluids. CFD simulations are performed using ANSYS FLUENT®. To compare the thermohydraulic performance of the system, the following assumptions are made:
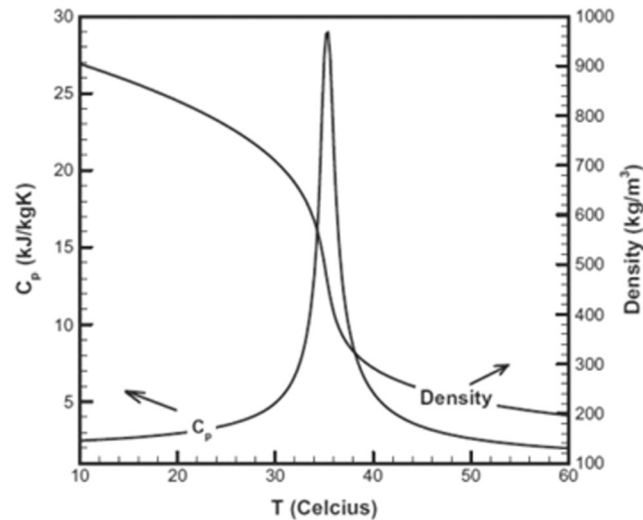
FIGURE 1 Thermal physical properties of supercritical CO_2 fluid at 8 MPa. Data from NIST[25]
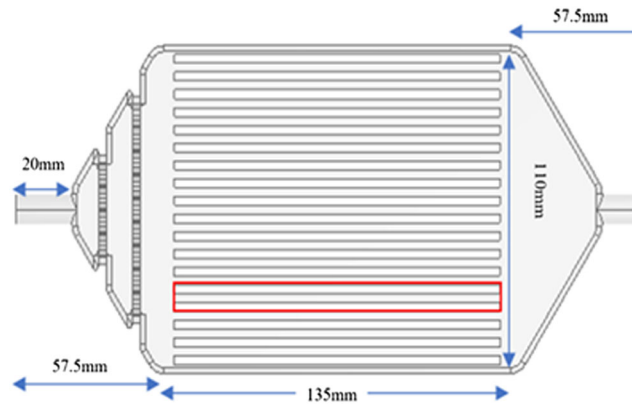

FIGURE 2 Heat sink dimensions [Colour figure can be viewed at wileyonlinelibrary.com]

- Cooling fluid is equally distributed in each of the channels in the heat sink.
- Uniform heat flux is applied to the top and bottom surfaces while side walls are adiabatic.
- The effects of radiation are neglected.
- The steady-state condition is achieved.
- The coolant can be modeled as a single-phase fluid.
- The contact losses are considered negligible between the fluid and the solid domain interfaces.
- Heat flux is uniformly dissipated on the channels surface.
- Thermal resistance between the heat source and the base of the heat sink is neglected.

2.1 | Physical model

The geometry of the heat sink is shown in Figures 2 and 3. The coolant passes through parallel rectangular channels and removes the heat from the top and bottom walls, on which electronics are glued and generate a constant heat flux, $\dot{q}$, on each wall.

Figure 3 illustrates details of the channel section. Following Sakanova et al.,[26] a single-layered channel heat sink (CHS) is used for this study with either water or s-CO_2 as the coolant.

The inlet conditions for water and CO_2 are shown in Table 2 and used as boundary conditions for the CFD model. Table 3 shows the dimensions of different channel geometries used for sensitivity analysis in CFD modeling. Case E is the actual channel dimensions of the existing industrial model.

The computational domain includes both fluid and solid regions. For the solid region, zero velocity is applied, and the thermal conductivity for the solid material, k = 237 W/(m K) for aluminum, is used.

The mass flow at the inlet is given, and the inlet temperature of both fluids is set as shown in Table 2. The outlet condition is pressure outlet, and the reference pressure at the outlet is set to zero. The heat source is defined at the top and bottom walls of the channel with a constant heat flux set to 2000 W/m². Assuming the heat loss from the sidewalls of the channel is negligible, the side walls are set as adiabatic.

2.2 | Mathematical model

To assess the cooling performance of a heat sink, the maximum and minimum temperatures at the heated surfaces as well as the pumping power required for coolant circulation inside the channels are studied based on the work of Sakanova et al.[26]
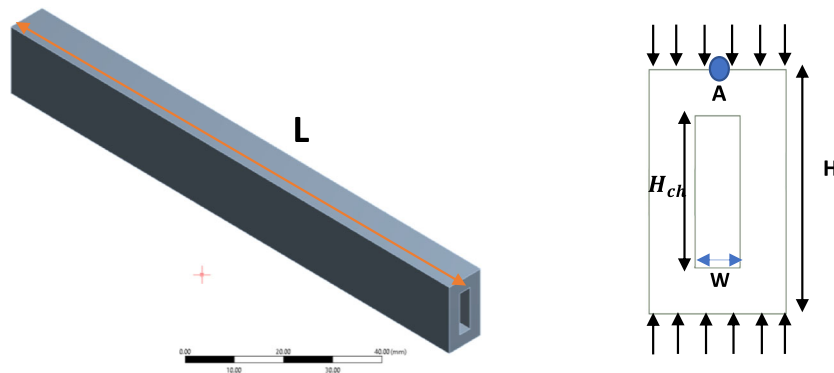

FIGURE 3 (Left) Single channel model and (right) dimensions of the channel cross section [Colour figure can be viewed at wileyonlinelibrary.com]

TABLE 2 Inlet conditions for water and s-CO_2

Inlet conditions	Water	s-CO_2
Tin (°C)	32	32
Pin (MPa)	0.2	8
m (kg/s)	0.004	0.004
P (kg/m³)	998	652.12
$\dot{q}$ (W/m²)	2000	2000

TABLE 3 Dimensions of one channel for CFD analysis

Dimensions	Case						
	A	B	C	D	E	F	G
D_h (mm)	1.50	2.75	3	3.75	4.6	5.30	5.45
W_{CH} (mm)	3	3	3	3	3	3	3
H_{ch} (mm)	1	2.5	3	5	10	24	30
L_{ch} (mm)	126	126	126	126	126	126	126
AR (H/W)	0.33	0.83	1	1.66	3.33	8	10

The cooling performance of channel or microchannel heat sink can be evaluated using the local heat transfer coefficient $h_{(x)}$ defined by Equation (1) as

$$h_{(x)} = \frac{\dot{q}}{T_{wall_{(x)}} - T_{bulk_{(x)}}} \tag{1}$$

where $\dot{q}$ is the prescribed constant heat flux applied at the top and bottom walls, $T_{wall_{(x)}}$ is the temperature of the centreline on the wall, shown in Figure 3 by point A, and $T_{bulk_{(x)}}$ is a fluid bulk temperature taken at the section along the channel length. Both temperatures are obtained via CFD simulation.

For a given channel, the hydraulic diameter is calculated by

$$D_h = \frac{2WH}{W + H} \tag{2}$$

where W and H are channel width and channel height, respectively, as depicted in Figure 3. The averaged Nusselt number, $\overline{Nu}$, can be calculated by using the averaged heat transfer coefficient, $\overline{h}$:

$$\overline{Nu} = \frac{\overline{h}.D_h}{k} \tag{3}$$

where k is the fluid thermal conductivity at inlet temperature.

2.3 | Thermal and hydraulic entrance length in the channel

Several studies showed that microchannel flow correlations are greatly linked to L_{th}, the thermal entrance length.[27,28] For a turbulent flow, this length does not exceed 20 times the channel hydraulic diameter (D_h). However, in the case of a laminar flow, the thermal length L_h is longer than the entrance thermal length for turbulent flow and is a linear unction of both Reynolds (Re) and Prandtl (Pr) numbers as shown in Equation (5). For a rectangular channel, the hydrodynamic entrance length (L_h) for laminar and turbulent flows is calculated using Equations (4) and (6), respectively[29]:

For turbulent flow:

$$\frac{L_{th}}{D_h} = \frac{L_h}{D_h} = 20 \tag{4}$$

$$L_{th} = 0.16 D_h Re Pr \tag{5}$$

$$L_h = 0.05 Re D_h \tag{6}$$

The required entrance length and Reynolds number for both water and CO_2 for the current geometry are shown in Table 4. It shows that the entrance length for laminar flow is much longer than the existing channel length of 126 mm. Hence, the flow will always be in the developing region when Reynolds is less than 2700. However, for CO_2, the Reynolds number is much higher, and the flow is turbulent. The entrance length for CO_2 is $x/D = 22.2$, beyond which the flow can be considered fully developed.

TABLE 4   Entrance length for water and CO_2, for m = 0.004 kg/s, AR = 3.33, $\dot{q} = 2000$ W/m^2

Entrance length	Water	CO$_2$
Thermal length required	1022 mm	90 mm
Hydrodynamic length required	58 mm	90 mm
Reynolds number	781	24,654

TABLE 5 Definition of flow regimes used for CFD calculations

Laminar flow	$Re < 2700$
Transitional flow	$2700 < Re < 3800$
Turbulent flow	$Re > 3800$

2.4 | Heat transfer coefficient and pressure drop

As presented in the previous sections, a CFD model is proposed, in laminar and turbulent regimes. Preliminary validation of calculations is conducted and compared with the experimental work of previous works,[29–31] and good agreement between both results is noted. As a result, the three regions for varying Reynolds numbers defined in Wang et al.[30] are used in this paper and are shown in Table 5.

The pressure drop, ΔP, for single phase channel flow is calculated by

$$\Delta P = 4 f L_{DP} \frac{\dot{m}^2}{2\rho Ac^2 D_h} \tag{7}$$

where f is the friction factor, L_{DP} the total length of the channel between inlet and outlet, $\dot{m}$ the mass flow rate, r the density, and Ac is the channel area. The experimental friction factor for hydrodynamically fully developed laminar flow is given in Equation (8). For transitional and turbulent regions, the friction factor is given by the Blasius equation, Equation (9).[31]

$$f = 64/\mathrm{Re} \tag{8}$$

$$f_{Bl} = 0.3164 \, \mathrm{Re}_{Dh}^{-0.25} \tag{9}$$

With a given ΔP, the pumping (PP) is described as

$$PP = \Delta P \frac{\dot{V}}{\eta} \tag{10}$$

$\dot{V}$ is the volume flow rate (m³/s) of cooling fluid in the channel and η is the pump efficiency.

2.5 | Governing equations and boundary conditions

The fluid flow and heat transfer in the channel are described using the governing equations for mass continuity Equation (11), conservation of momentum Equation (12), and energy for turbulent flow Equation (13).

$$\nabla.(\rho V) = 0 \tag{11}$$

$$\nabla(\rho VV) = \nabla(\mu \nabla V) - \nabla P + \rho g + F \tag{12}$$

$$\nabla.\left(\rho V C_p T\right) = \nabla(k \nabla T) \tag{13}$$

2.6 | Modeling, simulation method, and grid dependency check

For CFD simulations, different grids are used for mesh sensitivity analysis, depending on the flow and fluid conditions. For the laminar flow and the channel height of 10 mm, the mesh size is 0.5 mm on the X-axis for both solid and fluid regions. For the turbulent flow, the mesh size is 0.3 mm in the fluid region while the solid mesh size is kept at 0.5 mm (see Table 6). This parametric study allowed us to find that CFD results are grid-independent when the total element number exceeds 240×10^3 for the laminar flow and 470×10^3 for turbulent flow aiming for two parameters, that is, total pressure drop and outlet temperature. Mesh size is homogeneous along X-axis and presents a growth rate of 1.1 along Y and Z, to capture the sharp gradients within and at the boundary layer edges. The mesh size for other channel heights, for example, 30, 24, 5, 2.5, and 1 mm, is adapted accordingly. Figure 4 shows details of the meshing used for the calculation.

The discretization method applied for each fluid and flow regime is different and is shown in Table 7. For laminar flow, first-order upwind scheme and, for turbulent flow, second-order upwind scheme were used to discretize the convective terms. The second-order upwind scheme was used for discretizing dissipation terms in both laminar and turbulent regimes. The pressure and velocity are coupled using the COUPLED algorithm. The convergence criterion is set at 10^{-6} while the summation of normalized residuals in each control volume (CV) is kept below 10^{-9}. $k - \epsilon$ and $k - \omega$ were used and compared to select a proper solver and the latter was found as the preferred solver because the solution converged faster (see Table 6).

2.6.1 | Model validation results

Results of the proposed CFD model are also validated against the equations explained in Section 2.4 for two cases. First, three different channels with aspect ratios defined in Mehendafe et al.[16] are simulated where W/H is the aspect ratio given in Table 8. Then, the actual channel used in this paper with a constant aspect ratio of 3.3 with a variable mass

TABLE 6 Grid independency and mesh sensitivity analysis

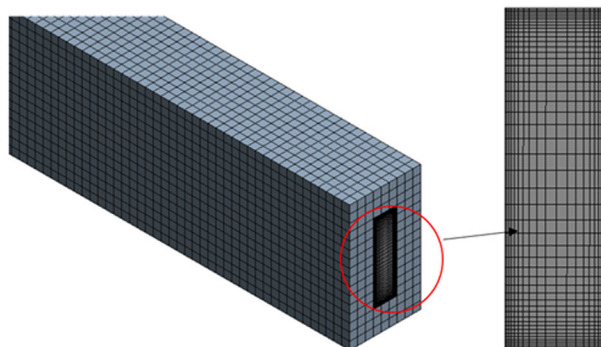| Case	Solver	Mesh elements	Convergence remarks/ iteration	Nx, Ny, and Nz for fluid	Total pressure drop (Pa)	Fluid outlet temp. (K)
A	Laminar	279,564	Converged	$252 \times 20 \times 20$	37	305.15
B	$k - \varepsilon$	510,912	Converged/935	$252 \times 40 \times 30$	780	305.2
	$k - \omega$		Converged/700			
C	$k - \varepsilon$	562,000	Converged/1550	$252 \times 45 \times 30$	784	305.3
	$k - \omega$		Converged/1200			
D	$k - \varepsilon$	618,200	Converged/1260	$252 \times 50 \times 30$	784	305.4
	$k - \omega$		Converged/1245			

FIGURE 4   Constructed mesh for the solid and fluid regions [Colour figure can be viewed at wileyonlinelibrary.com]

TABLE 7 Discretization of the CFD calculation

Parameter for discretization	Water	s-CO$_2$
Solver	SIMPLE	COUPLED
Conductivity	First-order upwind	Second order upwind
Dissipation	Second-order upwind	QUICK Scheme
Energy	First-order upwind	Second order upwind

TABLE 8 Validation of CFD model for laminar developing flow-$\dot{m} = 0.004$ kg/s, $(\dot{q}) = 2000$ W/m^2

Channel dimensions (mm)	W/H	Nu^{32}	Nu CFD	Error %	f^{32,33}	f CFD	Error%	Re
W 3 × H 3	1	7.78	7.58	8%	0.074	0.074	0	859
W 3 × H 2.5	1.2	7.58	5.77	23%	0.061	0.066	9%	1034
W 3 × H 1	3	7.62	8.1	6.1%	0.092	0.1	9%	976
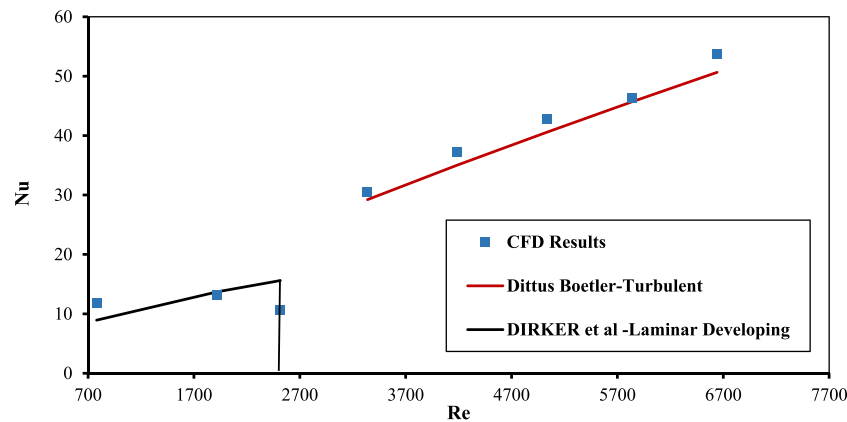
FIGURE 5 Validation of Nu number with literature and textbook,[32,33] variable flow rates (0.004–0.03 kg/s), channel AR = 0.33, and $\dot{q} = 2000$ W/m^2 [Colour figure can be viewed at wileyonlinelibrary.com]

flow rate is simulated. Figure 5 compares the numerical values of $\overline{Nu}$, averaged over the length of the channel, from CFD simulation for both laminar and turbulent flows against the existing correlations.[30,32] As illustrated, for Reynolds less than 2700 and above 3300, the CFD results are following the same trend as predicted by theoretical equations. The obvious change in the trend of Nu, and the increase with Re, as Reynolds exceeds 2700 marks a transition from laminar to the transitional region which is also expected.

The results of Nu from the CFD calculation in Table 8 show a maximum of 23% deviation from the equations used in the literature for the aspect ratio of 1.2. The Reynolds number for aspect ratio of 1.2 is in the transitional region, which can affect the CFD result. However, the other two channel aspect ratios are in good agreement with the literature with 8% and 1.2% deviation, respectively.

3 | RESULTS AND DISCUSSION

This section presents the results of the CFD analysis conducted on a single channel as shown in the previous sections. In reporting the results, we fix the global channel geometry and the heat input which are practical design constraints imposed by the industry partner. To conduct a parametric study, however, the numerical values of the coolant mass

flow rate, the aspect ratio, and the inlet temperature are systematically varied for both working fluids considered here. Dependent variables including heat transfer coefficient, pressure drop, and pumping power are investigated along with dimensionless numbers including f, Nu, and Re.

3.1 | Effect of mass flow rate

The thermal performance of a single channel with various mass flow rates is shown for both water and s-CO_2, in Figure 6, employing non-dimensional Nusselt number against Reynolds number. As seen, different trends are noted for different flow regimes. The Nu values for s-CO_2 at the minimum flow rate (A: 0.004 kg/s) are still 31 times higher than water in the channel under the same condition. The reason for such a significant difference is that s-CO_2 is near its critical region (high thermal capacity) and in a turbulent regime with a Reynolds number of around 32,000, which is also 40 times higher compared with the Reynolds of water, of around 800, at the same inlet temperature and mass flow rate. Moreover, the increasing water flow rate beyond 0.01 kg/s in one channel with an aspect ratio of 3.33 changes the flow regime from laminar to transitional and then turbulent. This phenomenon results in a change in the heat transfer coefficient for water, hence an abrupt change in Nu values is apparent. In the case of CO_2 in the supercritical region, the flow in the channel is always turbulent with the given mass flow rates, and the heat transfer coefficient monotonically increases with Re as anticipated.

Figure 7 illustrates the friction factor for both coolants in the same channel against the Reynolds number. As seen, the friction factor (f) for water is almost five times higher than that of s-CO_2 at the same mass flow rate of 0.004 kg/s (point A in the figure insert). The reason is that water is in a laminar regime while s-CO_2 flow is turbulent for the same flow rate. The lower density and viscosity of s-CO_2 result in a lower pressure drop compared with water. For Re values between 1920 and 3300, the transitional flow regime for water is noted.

By increasing the flow rate above 0.01 kg/s, the flow regime will change to turbulent resulting in lower friction factor values. The trend can be observed in the graph for water as marked laminar, transitional, or turbulent. The friction factor has a direct relationship with the power consumed by the pump or compressor, which is showing higher pumping power is required for water in comparison with s-CO_2.

Developing flow regions, either laminar or turbulent, are associated with higher heat transfer rates compared with the fully developed ones. Hence, as Figure 8 shows, water flow is designed to stay under developing conditions. However, even the developing Nu value for water is lower than the fully turbulent Nu value for the s-CO_2 flow in the same channel. Furthermore, Figure 8 shows the effect of critical temperature values for CO_2 on heat transfer. The 2°C decrease in s-CO_2 inlet temperature takes it to a subcritical state. While the heat transfer is almost halved for subcritical flow compared with the supercritical one, as s-CO_2 flow is still fully turbulent, it leads to higher Nu values, by an order
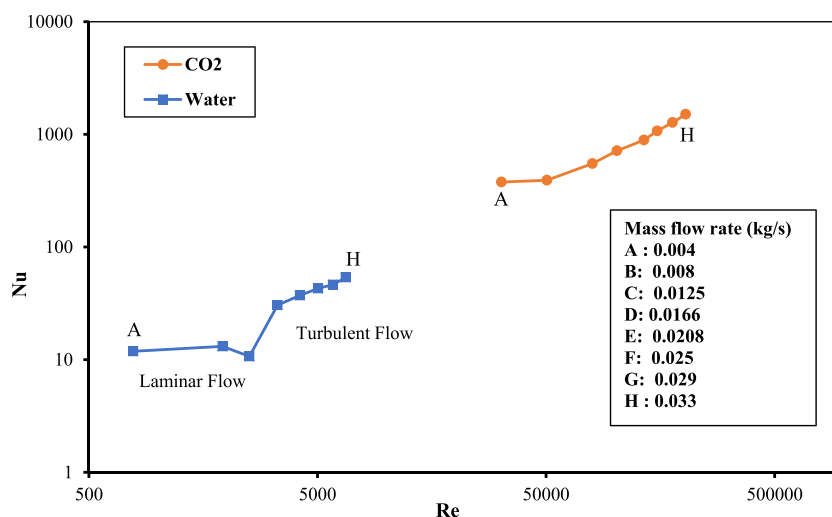

FIGURE 6 Nu variation for variable flow rate between 0.0044 kg/s to 0.033 kg/s, and AR = 3.33 [Colour figure can be viewed at wileyonlinelibrary.com]
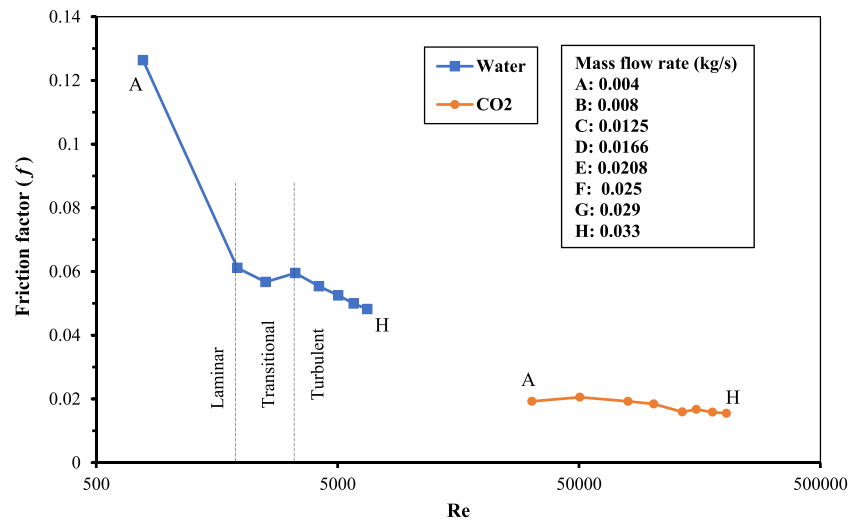
FIGURE 7 Results of friction factor for varying flow rate in the channel with AR = 0.33. [Colour figure can be viewed at wileyonlinelibrary.com]

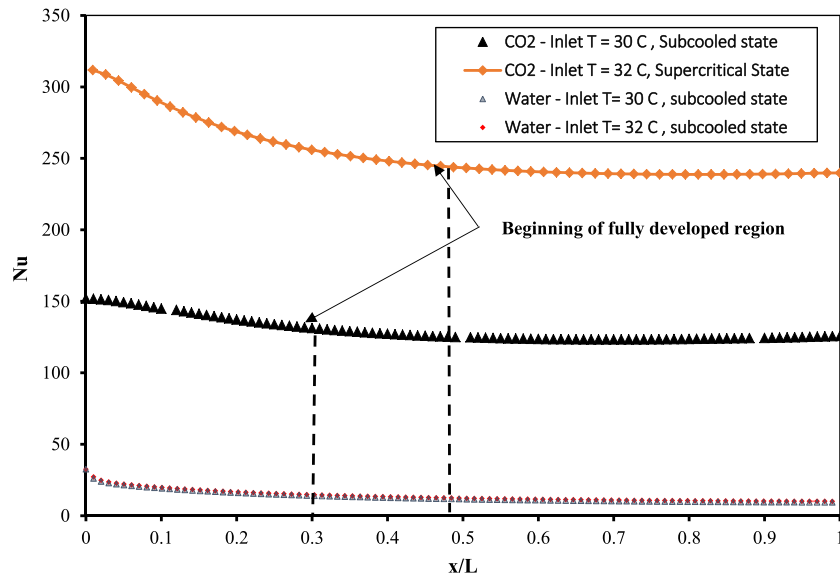**FIGURE 8** Comparison of *Nu* along the length of the channel for CO_2 and water at different inlet temperatures, with AR = 3.33 and ṁ = 0.004 kg/s [Colour figure can be viewed at wileyonlinelibrary.com]

of magnitude, compared with water at the same flow rate. One also notes that the s-CO_2 flow becomes fully developed when it reaches 30% and 40% of the channel length for subcooled and supercritical states, respectively. It brings home the point that the system can be further optimized to work with s-CO_2 through the use of shorter channels to avoid flow development thereby aiming at even higher heat transfer rates. Since newer versions of heat sinks are 3D printed, reducing their size allows to eliminate the current challenges of large components manufacturing, and brings gains in terms of manufacturing time and raw materials consumption.

Figure 9 shows the average heat transfer ($\bar{h}$) versus pumping power (PP) to circulate the cooling fluid, for different flow rates. The use of this graph is of great importance to the system designer. For a given pumping power, the heat transfer for s-CO_2 is significantly higher. As one would expect, the comparison does not have to rely on the same channel geometry but on the same pumping power. Hence, drawing a vertical line, at any point and crossing the plots would give the designer the difference in heat transfer between the two designs based on different working fluids. For example, with 0.1 W allowable pumping power, the heat transfer from s-CO_2 is three times higher than that of water. While
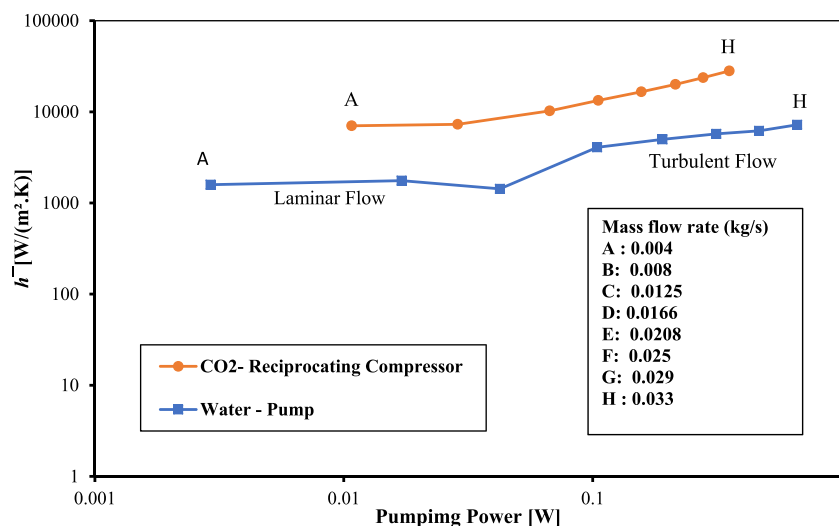
FIGURE 9 Comparison of average $\bar{h}$ and energy consumption for different flow rates, the inlet temperature 32°C, AR = 3.33 [Colour figure can be viewed at wileyonlinelibrary.com]

the use of Nu and f are informative, a design engineer would need to "select" a pump or compressor for a given heat duty. Another way to interpret this graph is to set a fixed heat transfer rate and then compare the required pumping power. The close case here is to aim at a heat transfer coefficient of about $7\ kW/m2$ for which both points A for s-CO$_2$ design and point H for a water-cooled design will be functional. Interestingly, the former, the s-CO$_2$ system, leads to 80 times lower pumping power.

3.2 | Effect of aspect ratio

To investigate the effects of the channel geometry, the numerical value of the channel height, *H*, is varied while the channel width, *W*, is kept constant. In general, a decrease in aspect ratio (*H/W*), while keeping the mass flow rate constant, increases the Reynolds number as the average velocity is increased thereby resulting in higher *Nu* values, in line with observations made by Sarkar.[34] The AR variation has a direct effect on the Nusselt and Reynolds numbers for both fluids. Water flow is laminar while thermally developing for Reynolds numbers between 300 and 1900, which corresponds to aspect ratios between 10 and 1, respectively. For *Re* values higher than 1900, the flow becomes transitional. As Figure 10 indicates, *Nu* for s-CO$_2$ is much higher than that of water and the value monotonically increases as the aspect ratio drops. For water, however, a different trend is observed when moving from B to A. This is because of a flow regime change from laminar to transitional in the channel. Comparing the two coolants, one observes a superior performance with s-CO$_2$. The Nusselt number for s-CO$_2$ is 10 times higher than that of water when the aspect ratio is 10 (point G) and it is 33.3 times higher than that of water when the aspect ratio is 0.33 (point A).

Figure 11 demonstrates the effect of aspect ratio on the pressure drop, presented in terms of friction factor, as a function of Reynolds number, for both water and s-CO$_2$. The friction factor for s-CO$_2$ is lower when compared with water at the same flow rate. The lowest aspect ratio of 10 yields the highest *f* value for both fluids as expected. As the aspect ratio increases the Reynolds number increases accordingly resulting in lower friction factors. The friction factor shows the same trend as described in Wang et al.[30] For s-CO$_2$, the flow is always turbulent; thus, for the same aspect ratio, the friction factor is always lower compared with that of water.

3.3 | Effect of critical point

The authors investigate the effects of critical points on the heat transfer performance of the two coolants for a set aspect ratio by plotting local heat transfer in the streamwise direction. This section investigates the effects of operating conditions when they push CO$_2$ to a subcritical state for instance when the CO$_2$ inlet temperature is reduced to 30°C.
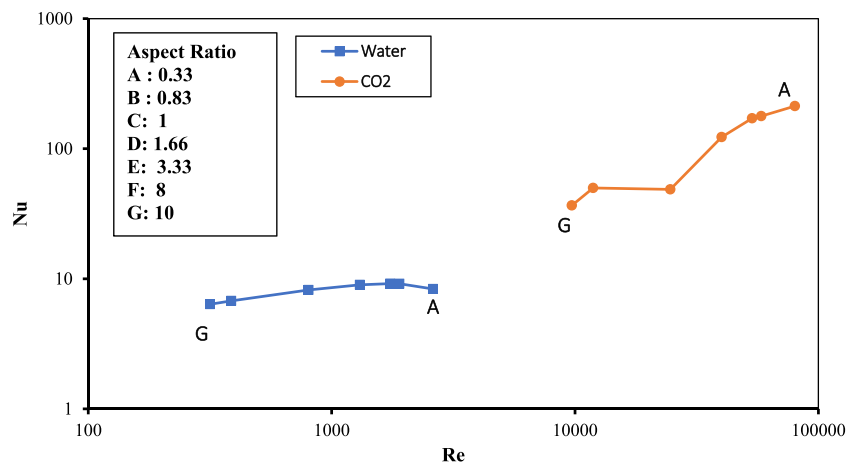
FIGURE 10   Effect of aspect ratio on *Nu* with ṁ = 0.004 kg/s [Colour figure can be viewed at wileyonlinelibrary.com]
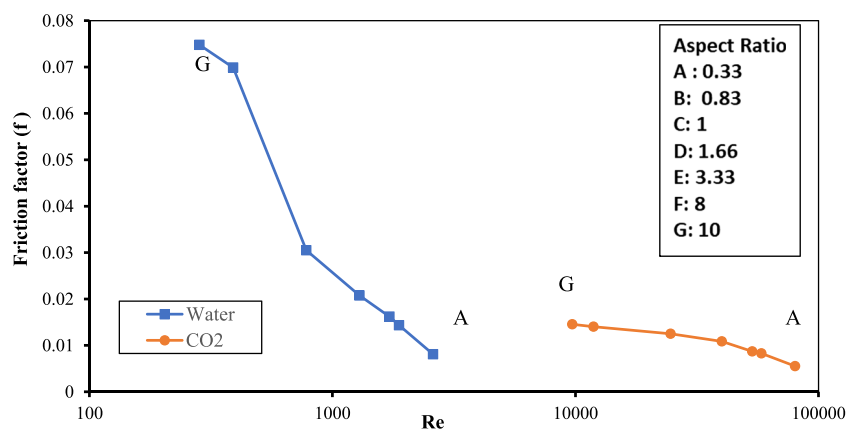

FIGURE 11   Friction factor versus *Re* for different aspect ratios at ṁ = 0.004 kg/s [Colour figure can be viewed at wileyonlinelibrary.com]

Figures 12 and 13 plot the heat transfer coefficient versus pumping power for both coolants while the CO_2 state is supercritical in the former and subcritical in the latter. In both cases, for the same pumping power, CO_2 leads to a higher heat transfer rate. Moreover, another way of reading the graphs is to conclude that for the same pressure drop, the heat transfer is higher with s-CO_2 compared with that of water. Finally, one notes a lower s-CO_2 heat transfer coefficient for the subcritical state.

4 | SUMMARY AND CONCLUSION

The purpose of this study is to explore the use of CO_2 as a replacing coolant instead of Water for microchannel heat sinks (MCHS). In this regard, the thermal and hydraulic entrance length, aspect ratio, and mass flow rate have a significant effect on thermal performance and pumping power of mini channels specifically if the coolant (e.g., CO_2) properties vary by pressure and temperature inlets. Such detailed investigation of parameters for s-CO_2 application in heat sinks has not been properly addressed in the previous reports.

In this report, a comparison has been made between the thermal and hydraulic characteristics of MCHS with both traditional and proposed coolants (water and s-CO_2). The results in terms Nusselt number (*Nu*), friction factor, heat transfer coefficient (*h*) and power consumption against variation of channel aspect ratio (AR), and mass flow rate (ṁ) were reported. Moreover, the effect of two different inlet temperatures, that is, T = 30°C and T = 32°C on the
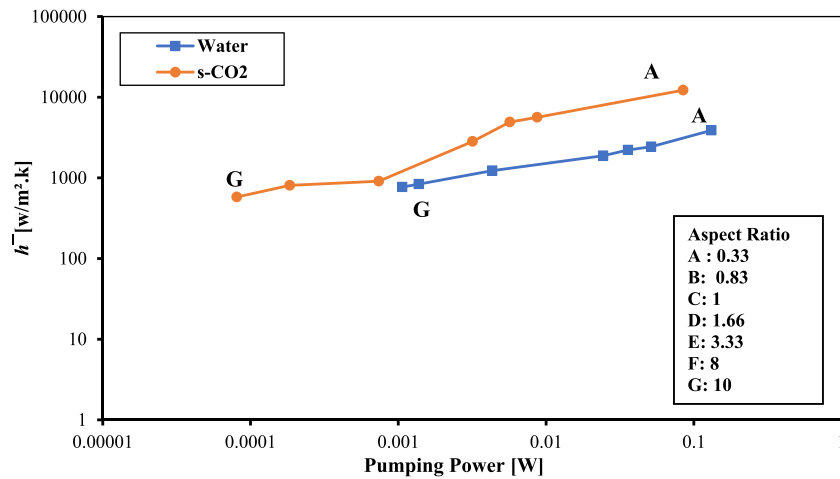
FIGURE 12   Effect of aspect ratio on heat transfer and power consumption in a rectangular channel for water and s-CO_2, $T_{in} = 32°C$, $\dot{m} = 0.004\,kg/s$ [Colour figure can be viewed at wileyonlinelibrary.com]

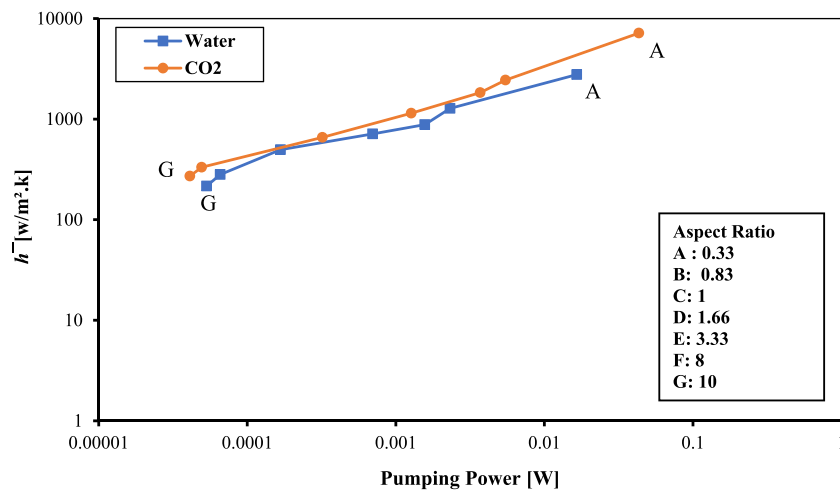**FIGURE 13**   Effect of aspect ratio on heat transfer and power consumption in a rectangular channel with $T_{in} = 30°C$, $\dot{m} = 0.004\,kg/s$, for water and s-CO_2 [Colour figure can be viewed at wileyonlinelibrary.com]

performance of CO_2-cooled mini channel and power consumption, is discussed. The main conclusions drawn from this study are

- The average surface Nusselt number for s-CO_2 in one channel is almost 10 times more than that of water due to the higher Reynolds number for the s-CO_2 in one mini-channel.
- The average heat transfer coefficient for s-CO_2 for a given aspect ratio of 0.33 can reach up to 31 times higher than that of water at the same inlet temperature. As the specific heat capacity and viscosity of s-CO_2 are lower near the pseudocritical region, the heat transfer coefficient for s-CO_2 is 4.5 times higher at the same flow rate compared with water.
- The friction factor results are discussed for both fluids and it is shown that s-CO_2 has a much lower friction factor than water for all considered cases regardless of the mass flow rate and channel aspect ratio. The friction factor for low AR (0.33) is calculated as 0.005 and 0.008 for s-CO_2 and water, respectively, while at AR = 10, the values are 0.014 and 0.070, respectively.
- It is noted that the pumping power for s-CO_2 is dependent on the inlet temperature thus the state of s-CO_2. The reported results demonstrated in sub-cool condition at T = 30°C and mass flow rate of 0.004 kg/s, pumping power

(PP) for water (AR = 0.33) is almost 1.3 times more than PP consumed for s-CO_2, while at AR = 10, this value for s-CO_2 is 2.6 times higher than of water. This result clearly shows the effect of the thermal and hydraulic entrance since the change of AR changes Reynolds number in mini-channels thus the pumping power.

5 | FUTURE WORKS

As a prospect and since the newer versions of heat sinks are 3D printed, the effect of the surface roughness and pores due to the manufacturing process will be taken into account via experimental and further numerical studies in our near future works. Additionally, the experimental work will be conducted to optimize the diffusers and divergent section of the heat sink which plays a crucial role in the thermal performance of the MCHS due to its effect on the flow distribution. This study has also investigated the effect of two key variables on the thermal performance of a single mini-channel as well as the effect of entrance length on the heat transfer and pumping power of coolants. Future work will benefit from the results of this study to simulate and optimize a complete 3D model of a pre-designed mini-channel heat sink with consideration of flow distribution through channels via diffusers for both s-CO_2 and water coolants.

In summary, while the heat transfer is higher with CO_2, the pressure drop is lower compared with that of water. This result is crucial in industrial applications as it favors the use of s-CO_2 as a cooling fluid with great potential to improve cooling performance while reducing the overall weight of the system.

CONFLICT OF INTEREST
This work does not have any conflicts of interest.

AUTHOR CONTRIBUTIONS
Navid Dehdashti Akhavan: Conceptualization; investigation; writing. **Foued Abroug:** Conceptualization; software; supervision; writing. **Lionel Arnaud:** Formal analysis; methodology; review. **Kamel Hooman:** Supervision; visualization; writing – reviewing & editing.

NOMENCLATURE

AR	aspect ratio (H_{ch}/W_{ch})
A_c	channel area (m^2)
Cp	specific heat capacity ($J\ kg^{-1}\ °C^{-1}$)
$\mathcal{D}h$	hydraulic diameter (mm)
f	friction factor
H_{ch}	height of channel (mm)
h_x	local heat transfer coefficient ($W\ m^{-2}\ °C^{-1}$)
$\overline{h}$	average heat transfer coefficient ($W\ m^{-2}\ °C^{-1}$)
k	thermal conductivity ($m^{-1}\ K^{-1}$)
L_{ch}	length of channel (mm)
L_{th}	thermal length (mm)
L_h	hydraulic length (mm)
m	mass flow rate ($kg\ s^{-1}$)
$\overline{Nu}$	averaged Nusselt number
P	total pressure (MPa)
Pin	inlet pressure (MPa)
ΔP	pressure drop (kPa)
Pr	Prandtl number
PP	pumping power (W)

Q heating load (W)

$\dot{Q}$ heat flux (W m^{-2})

Re   Reynolds number

Tin inlet temperature (°C)

T   temperature (°C)

$T_{wall(x)}$ wall temperature on centerline (°C)

$T_{bulk(x)}$ fluid bulk temperature at the section of the channel (°C)

ΔT change in coolant temperature from inlet to outlet (°C)

V   velocity vector (m s^{-1})

$\dot{V}$ volumetric flow rate (m^3 s^{-1})

W_{ch} width of the channel (mm)

GREEK SYMBOLS

ρ density (kg m^{-3})

η efficiency

μ dynamic viscosity (m^{-1} s^{-1})

ORCID

Navid Dehdashti Akhavan ⓘ https://orcid.org/0000-0003-3299-2684

Kamel Hooman ⓘ https://orcid.org/0000-0003-0282-7960

REFERENCES

1. Taher H, Al-Zuhair S, Al-Marzouqi A, Haik Y, Farid M. Growth of microalgae using CO_2 enriched air for biodiesel production in supercritical CO_2. *Renew Energy*. 2015;82:61-70. doi:10.1016/j.renene.2014.08.013

2. Dostal V, Driscoll M, Hejzlar P. A supercritical carbon dioxide cycle for next generation nuclear reactors. 2004. https://www.academia.edu/download/60925385/A_Supercritical_Carbon_Dioxide_Cycle_for20191016-56157-48a23k.pdf (Accessed June 1, 2021).

3. Hu L, Chen D, Huang Y, et al. Investigation on the performance of the supercritical Brayton cycle with CO_2-based binary mixture as working fluid for an energy transportation system of a nuclear reactor. *Energy*. 2015;89:874-886. doi:10.1016/j.energy.2015.06.029

4. Kizilkan O. Performance assessment of steam Rankine cycle and sCO_2 Brayton cycle for waste heat recovery in a cement plant: a comparative study for supercritical fluids. *Int J Energy Res*. 2020;44:12329-12343. doi:10.1002/er.5138

5. Tamura T, Yakumaru Y, Nishiwaki F. Experimental study on automotive cooling and heating air conditioning system using CO_2 as a refrigerant. *Int J Refrig*. 2005;28(8):1302-1307. doi:10.1016/j.ijrefrig.2005.09.010

6. Cabeza LF, de Gracia A, Fernández AI, Farid MM. Supercritical CO_2 as heat transfer fluid: a review. *Appl Therm Eng*. 2017;125:799-810. doi:10.1016/j.applthermaleng.2017.07.049

7. Li H, Zhang Y, Zhang L, Yao M, Kruizenga A, Anderson M. PDF-based modeling on the turbulent convection heat transfer of supercritical CO_2 in the printed circuit heat exchangers for the supercritical CO_2 Brayton cycle. *Int J Heat Mass Transf*. 2016;98:204-218. doi:10.1016/j.ijheatmasstransfer.2016.03.001

8. Rochau GE. Operation and analysis of a supercritical CO_2 Brayton cycle. n.d. doi:10.2172/984129

9. Wright SA, Radel RF, Vernon ME, Pickard PS, Rochau GE. Operation and analysis of a supercritical CO_2 Brayton cycle. Albuquerque, NM, and Livermore, CA (United States). 2010. doi:10.2172/984129

10. Utamura M, Hasuike H, Ogawa K, et al. Demonstration of supercritical CO2 closed regenerative Brayton cycle in a bench scale experiment. *Proc. ASME Turbo Expo, American Society of Mechanical Engineers Digital Collection*. 2012;155-164. doi:10.1115/GT2012-68697

11. Gillot C, Bricard A, Schaeffer C. Single- and two-phase heat exchangers for power electronic components. *Int J Therm Sci*. 2000;39:826-832. doi:10.1016/S1290-0729(00)00278-7

12. Chu WX, Li XH, Ma T, Chen YT, Wang QW. Experimental investigation on SCO_2-water heat transfer characteristics in a printed circuit heat exchanger with straight channels. *Int J Heat Mass Transf*. 2017;113:184-194. doi:10.1016/j.ijheatmasstransfer.2017.05.059

13. Aprea C, Maiorino A. An experimental evaluation of the transcritical CO_2 refrigerator performances using an internal heat exchanger. *Int J Refrig*. 2008;31(6):1006-1011. doi:10.1016/j.ijrefrig.2007.12.016

14. Llopis R, Nebot-Andrés L, Cabello R, Sánchez D, Catalán-Gil J. Évaluation expérimentale d'une installation frigorifique transcritique au CO_2 avec un sous-refroidissement mécanique dédié. *Int J Refrig*. 2016;69:361-368. doi:10.1016/j.ijrefrig.2016.06.009

15. Sarkar J, Bhattacharyya S, Gopal MR. Optimization of a transcritical CO_2 heat pump cycle for simultaneous cooling and heating applications. *Int J Refrig*. 2004;27:830-838. doi:10.1016/j.ijrefrig.2004.03.006

16. Mehendafe SS, Jacobi AM, Shah RK. Fluid flow and heat transfer at micro- and meso-scales with application to heat exchanger design. *Appl Mech Rev*. 2000;53(7):175-193. doi:10.1115/1.3097347

17. Dixit T, Ghosh I. Review of micro- and mini-channel heat sinks and heat exchangers for single phase fluids. *Renew Sustain Energy Rev*. 2015;41:1298-1311. doi:10.1016/j.rser.2014.09.024

18. Xu XY, Wang QW, Li L, Ekkad SV, Ma T. Thermal-hydraulic performance of different discontinuous fins used in a printed circuit heat exchanger for supercritical CO_2. *Numer Heat Transf Part A Appl*. 2015;68(10):1067-1086. doi:10.1080/10407782.2015.1032028

19. Kandlikar SG, Colin S, Peles Y, et al. Heat transfer in microchannels—2012 status and research needs. *J Heat Transfer*. 2013;135(9): 091001. doi:10.1115/1.4024354

20. Tuckerman DB, Pease RFW. High-performance heat sinking for VLSI. *IEEE Electron Device Lett*. 1981;2(5):126-129. doi:10.1109/EDL. 1981.25367

21. Martins C. __EP1903293A2 automobile heat exchanger s-CO2.pdf, EP 1903293A2. 2008.

22. Ducoulombier M, Colasson S, Haberschill P, Tingaud F. Charge reduction experimental investigation of CO_2 single-phase flow in a horizontal micro-channel with constant heat flux conditions. *Int J Refrig*. 2011;34(4):827-833. doi:10.1016/j.ijrefrig.2011.01.013

23. Hitachi T, Gohara H, Nagaune F. Direct liquid cooling IGBT module for automotive applications. 2012.

24. Rao NT, Oumer AN, Jamaludin UK. State-of-the-art on flow and heat transfer characteristics of supercritical CO_2 in various channels. *J Supercrit Fluids*. 2016;116:132-147. doi:10.1016/J.SUPFLU.2016.05.028

25. Lemmon EW, Huber ML, McLinden MO. NIST Standard Reference Database 23: reference fluid thermodynamic and transport properties-REFPROP, Version 8.0. n.d. https://www.nist.gov/publications/nist-standard-reference-database-23-reference-fluid-thermodynamic-and-transport-0 (Accessed June 10, 2021).

26. Sakanova A, Yin S, Liu Y, et al. Heatsink design for high power density converter in aircraft applications: parameter sensitivity analysis. In: *2015 International Conference on Electrical Systems for Aircraft, Railway, Ship Propulsion and Road Vehicles (ESARS)*. 2015:1-6. doi:10.1109/ESARS.2015.7101419

27. Sakanova A, Yin S, Zhao J, Wu JM, Leong KC. Optimization and comparison of double-layer and double-side micro-channel heat sinks with nanofluid for power electronics cooling. *Appl Therm Eng*. 2014;65(1-2):124-134. doi:10.1016/j.applthermaleng.2014.01.005

28. Meyer JP, Everts M. Single-phase mixed convection of developing and fully developed flow in smooth horizontal circular tubes in the laminar and transitional flow regimes. *Int J Heat Mass Transf*. 2018;117:1251-1273. doi:10.1016/j.ijheatmasstransfer.2017.10.070

29. Everts M, Meyer JP. Laminar hydrodynamic and thermal entrance lengths for simultaneously hydrodynamically and thermally developing forced and mixed convective flows in horizontal tubes. *Exp Therm Fluid Sci*. 2020;118:110153. doi:10.1016/j.expthermflusci.2020. 110153

30. Wang C, Gao P, Tan S, Wang Z, Xu C. Experimental study of friction and heat transfer characteristics in narrow rectangular channel. *Nucl Eng des*. 2012;250:646-655. doi:10.1016/j.nucengdes.2012.06.029

31. Muzychka YS, Ghobadi M. Measurement and analysis of laminar heat transfer coefficients in micro and mini-scale ducts and channels. *Heat Transf Eng*. 2016;37(11):938-946. doi:10.1080/01457632.2015.1098054

32. Dirker J, Meyer JP, Garach DV. Inlet flow effects in micro-channels in the laminar and transitional regimes on single-phase heat transfer coefficients and friction factors. *Int J Heat Mass Transf*. 2014;77:612-626. doi:10.1016/j.ijheatmasstransfer.2014.05.048

33. Shah ALLRK. *Laminar Flow Forced Convection in Ducts*. Elsevier; 1978. doi:10.1016/c2013-0-06152-x

34. Sarkar J. Improving thermal performance of micro-channel electronic heat sink using supercritical CO_2 as coolant. *Therm Sci*. 2019; 23(1):243-253. doi:10.2298/TSCI161110030S